IOP Publishing Modelling and Simulation in Materials Science and Engineering

Modelling Simul. Mater. Sci. Eng. **23** (2015) 055006 (24pp) doi:10.1088/0965-0393/23/5/055006

Field theory and diffusion creep predictions in polycrystalline aggregates

A Villani[1], E P Busso[2] and S Forest[1]

[1] Centre des Matériaux, MINES ParisTech, UMR CNRS 7633, France
[2] ONERA, General Scientific Directorate, Palaiseau, France

E-mail: samuel.forest@mines-paristech.fr

Received 4 August 2014, revised 31 March 2015
Accepted for publication 8 April 2015
Published 22 May 2015

Abstract

In polycrystals, stress-driven vacancy diffusion at high homologous temperatures leads to inelastic deformation. In this work, a novel continuum mechanics framework is proposed to describe the strain fields resulting from such a diffusion-driven process in a polycrystalline aggregate where grains and grain boundaries are explicitly considered. The choice of an anisotropic eigenstrain in the grain boundary region provides the driving force for the diffusive creep processes. The corresponding inelastic strain rate is shown to be related to the gradient of the vacancy flux. Dislocation driven deformation is then introduced as an additional mechanism, through standard crystal plasticity constitutive equations. The fully coupled diffusion-mechanical model is implemented into the finite element method and then used to describe the biaxial creep behaviour of FCC polycrystalline aggregates. The corresponding results revealed for the first time that such a coupled diffusion-stress approach, involving the gradient of the vacancy flux, can accurately predict the well-known macroscopic strain rate dependency on stress and grain size in the diffusion creep regime. They also predict strongly heterogeneous viscoplastic strain fields, especially close to grain boundaries triple junctions. Finally, a smooth transition from Herring and Coble to dislocation creep behaviour is predicted and compared to experimental results for copper.

Keywords: stress-diffusion coupling, vacancy diffusion, creep, polycrystal, crystal plasticity, finite element simulations, Nabarro-Herring

(Some figures may appear in colour only in the online journal)

1. Introduction

In crystalline metallic materials, the two main elementary creep mechanisms are crystallographic slip produced by dislocation glide and the deformation associated with vacancy

diffusion. As far as vacancies are concerned, two mechanisms are known: Coble creep, where vacancies diffuse along grain boundaries, and Herring-Nabarro creep [1], where vacancies diffuse through the bulk material. They operate, respectively, at low and high homologous temperatures. Vacancy diffusion can induce permanent deformations in the material, which raises the question as to how the corresponding strain rate can be related to the vacancy flux at the scale of individual grains.

Continuum mechanics is embodied by the deformation of material lines drawn on a deforming specimen. When such lines are too blurred due to severe diffusion processes, standard continuum mechanics fails as it is unable to describe such material behaviour. In this work, it will be shown that continuum mechanics can still be used as a compromise between detailed atomistic analysis and field theory when the blurring of material lines is not too severe, as mentioned by Berdichevsky and coworkers [2]. In addition to these material point considerations, polycrystal modelling poses several challenges. In particular, grain boundaries introduce a geometrical discontinuity, and provide the main driving force for diffusive creep processes.

In the literature, two classes of models can generally be found for diffusion creep: marker based models [3] and lattice based models [4, 5]. In the first class, the existence of indestructible entities is assumed, which are tied to the material and convect with it, such that the definition of strain remains possible. In lattice based models, the creep deformation is assumed to be linked to lattice based mechanisms, such as site creation/annihilation and diffusion of species in the lattice. In [5], the authors develop a model that accounts for the plastic deformation in grain boundary zones of finite width, but not in the bulk. In their work, the plastic deformation rate is assumed to be proportional to a sink term in the vacancy diffusion equation, and to be only active in the grain boundary region. Their model was later extended to account for grain boundary migration, using a level-set method [6]. To our knowledge, Berdichevsky *et al* [2] were the first to relate the viscoplastic deformation rate to the gradient of the vacancy flux, see equations (60) and (62) in [2]. In [7 and 8], the plastic strain rate is postulated as the symmetric part of the vacancy flux gradient, and the driving force arises from stress dependent boundary conditions imposed for the vacancy concentration. This formulation has also been used in [9], and is generally not applicable to a generic polycrystalline simulation. It is only recently that Mishin and coworkers [10] combined the two models and adopted a non-classical approach to account for grain boundaries migration. The authors identified three minimum ingredients required for creep modelling: a thermodynamic framework accounting for lattice site evolution, a model of microstructure evolution and an appropriate set of kinetics equations. Their model was applied to an elementary bicrystal with a symmetrical grain boundary. Other important contributions made on diffusion creep are those from [11–14], in which creep equations for a solid are derived with a continuous distribution of vacancy sinks and sources, associated, for instance, with dislocation climb mechanisms.

Classically, mechanical models are built using representative volume elements (RVE), whereby stress or strain heterogeneities are ignored or averaged. However, these heterogeneities contribute strongly to the behavior of the material, and polycrystalline aggregates simulations are now relied upon in order to obtain intragranular stress and deformation fields. It is known that heterogeneities originate from elastic anisotropy, crystallographic slip [15], and play a major role in crack nucleation [16, 17]. In [18], the transport equations for dislocations are complemented to account for climb mediated by diffusion processes, at the scale of precipitates. In turn, the plastic strain rate tensor is extended to incorporate this climb kinematics. However, in these works, the heterogeneities arising from the gradient of the vacancy flux are not accounted for.

The objective of the present work is to describe strain fields inside the grains arising from both diffusion processes and dislocation slip in a polycrystal subject to constant applied stress. In the present paper, the set of processes and associated equations necessary for a field theory of diffusional creep, where the diffusion creep viscoplastic deformation rate is related to the gradient of the vacancy flux, will be presented. This work is conducted at the meso-scale, with a detailed description of concentration and displacement fields inside a polycrystalline element, and with an explicit geometrical description of grains and grain boundaries. Fully coupled diffusion creep-crystal plasticity simulations of polycrystalline aggregates, including the effects of the vacancy flux gradient, are presented for the first time. The proposed framework encompasses Herring, Coble and dislocation creep mechanisms at the local intergranular and intragranular levels.

The first section is dedicated to the formulation of the creep kinetics in the spirit of Berdichevsky's work, and the diffusion induced creep strain-rate tensor is identified as the deviatoric and symmetric part of the gradient of the vacancy flux. Then, a chemical-mechanical coupled framework is developed from which Herring's diffusion relation [1] is naturally recovered, thus yielding the correct overall creep driving forces. In the proposed formulation, creep processes start naturally by applying mechanical boundary conditions on a polycrystal. It is assumed for simplicity that any grain boundary motion can be neglected.

In the second part, finite element (FE) creep simulations of polycrystalline copper are conducted using diffusion data available in the literature to predict the average creep strain rates. Then, the FE results are compared to classic analytical solutions [19], and the numerical treatment of a grain boundary is emphasized and compared to the literature [5, 8]. In the present work, grain boundaries are first treated with Dirichlet conditions; then, grains and grain boundaries are described by phase-field like variables [20]. Finally, crystal plasticity [21] is introduced as an additional deformation mechanism: incompatibilities arising close to grain boundaries modify the stress state which, in turn, influences the vacancy flux.

Cartesian coordinates will be used throughout the paper. Vectors will be denoted by $\underline{\boldsymbol{v}}$, second order tensors by $\underset{\sim}{\boldsymbol{\sigma}}$, and fourth order tensors by $\underset{\approx}{\boldsymbol{\Lambda}}$.

2. Kinetics of vacancy diffusion induced creep in crystals

2.1. Definition of a material point in the presence of diffusion

The pioneering work carried out by Cahn and Larché in the 70's and 80's [4, 22] introduced the notion of network to deal with some of the problems mentioned in the introduction. One would then think of a material point as a collection of lattice sites. A second possible definition would be to consider the material point as a collection of atoms. Indeed, the material lines of continuum mechanics, used for instance for strain field measurements, will not be drawn on the lattice in such case but rather on the atoms themselves. The two distinct notions are illustrated in figure 1. A material point based on the lattice definition would be, for instance, that represented by the black square in the figure. It is clear that the black square would distort (i.e. deform) in an irreversible manner if the number of lattice sites it contains would change. This would only occur if vacancies could either be generated or annihilated within the square. In contrast, a material point definition based on a group of atoms, such as those shown in red in figure 1, implies that an inhomogeneous diffusion of vacancies would be sufficient to produce a permanent deformation without the need to either generate or annihilate vacancies. Such is the case for the permanent shear deformation experienced by the material point (or element) defined by the red atoms in figure 1. In this work, the definition of the material point as a

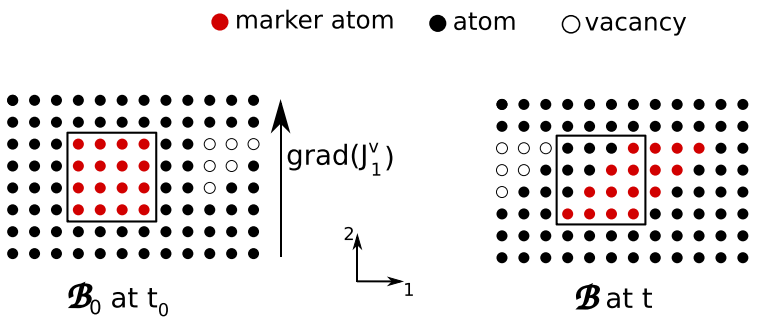

Figure 1. In this schematic illustration, the atoms of a material point at $t = 0$ are represented by red dots. Due to an imposed gradient of the vacancy flux, $\frac{\partial J_1^v}{\partial x_2} \neq 0$, the vacancies move from right to left, accompanied by an opposite motion of atoms. Here, the material element is sheared whereas the lattice volume element denoted by the box remains unchanged. In reality, the picture is only correct at a much larger scale than that of the present figure where just a few atoms are represented. Larger volume elements must be considered than that represented here.

collection of atoms will be adopted. The motivation for choosing the marker-based definition of a material point is the increasing use of strain field measurement methods in experimental mechanics based on deposited grids or patterns. In the fiducial grid sketched in figure 2, the measured strains do not refer to lattice based volume elements but rather to a collection of atoms coinciding, at least partially, with the deposited lines or points of the grid. Simulations of the type presented in the present work will be necessary for a quantitative interpretation of high resolution strain field measurements at high temperature and high in metallic polycrystals. This implies that the analysis presented in this work will be based on the following hypotheses:

- The positions of the atoms and vacancies are constrained by the lattice of the crystalline solid, i.e. they can only occupy substitutional sites in the crystalline lattice. Also, the creation and annihilation of lattice sites associated with defects like climbing dislocations are not considered for simplicity. The coupling between vacancy diffusion and a continuum description of dislocation climb was addressed in the references [14, 18].
- The volume element associated with the material point, V, is a bounding box encompassing this collection of atoms and any vacancies which may be trapped inside. This is the so—called marker—based definition of the material volume element.
- The diffusion processes should not be too severe for the material lines to keep their identity (see figure 2). Copper is well–suited for the present treatment. For instance in [23], experiments show a transition in creep behaviour from diffusion creep to dislocation creep at half the melting temperature (that is, as low as ∼700 K), for a grain size of a few tens of microns.
- Direct exchange between atoms does not occur. Any atom motion is accompanied by an opposite motion of a vacancy. This is a frequent assumption, and its justification lies on the fact that a direct exchange between substitutional atoms is energetically more expensive than when involving vacancies [24].

The latter assumption applies mainly to material volume elements in the grain's interior. The hypothesis of absence of site sources and sinks will be relaxed in the case of grain boundary regions.

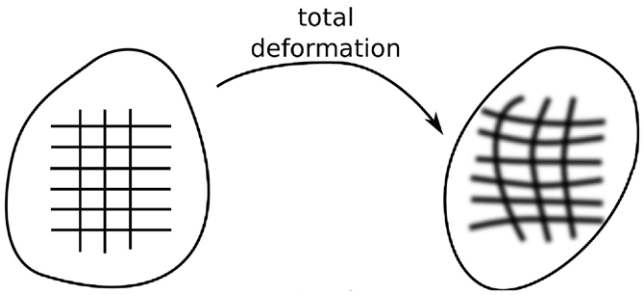

Figure 2. Dissolution of the reference lines in case of diffusion, drawn on a deforming body. From left to right, both straining and diffusion take place. Blurring occurs, but the lines keep their identity, thus allowing for the definition of a strain field to be made.

2.2. Coupling creep deformation and the gradient of the vacancy flux

In the following section, the considered species are atoms and vacancies, denoted with a superscript, k, equal to either a (atoms), or, v (vacancies). The reference configuration of the body is denoted by $\mathcal{B}_0$, made of material points $\mathcal{M}$, occupying the initial spatial position, $\underline{\boldsymbol{X}}$. In the current configuration at time, t, the body is denoted by $\mathcal{B}$, and its material points are located at, $\underline{\boldsymbol{x}}$. The function $\underline{\boldsymbol{x}} = \chi_u(\underline{\boldsymbol{X}}, t)$ maps the material points to the current configuration at time t. The following quantities are defined at each material point, $\mathcal{M}$:

- $n^{\#}(\underline{\boldsymbol{x}}, t)$ is the mole number of substitutional sites per unit volume [mol.m^{-3}] in the current state.
- $N^{\#}(\underline{\boldsymbol{X}})$ is the mole number of substitutional sites per unit volume [mol.m^{-3}] in the reference state.
- $n^k(\underline{\boldsymbol{x}}, t)$ is the mole number of substitutional species k per unit volume [mol.m^{-3}] in the current state.
- $N^k(\underline{\boldsymbol{X}})$ is the mole number of substitutional species k per unit volume [mol.m^{-3}] in the reference state.
- $c^k(\underline{\boldsymbol{x}}, t) = \frac{n^k}{n^{\#}}$ is the fraction of sites occupied by species k in the current state.

Furthermore, the network constraint imposes that

$$\sum_k n^k = n^{\#} \ . \tag{2.1}$$

In this subsection, the crystalline lattice is supposed fixed in space with respect to the observer and rigid [25]. Elastic straining of the lattice will be added later on. In the proposed analysis, interaction between vacancy and defects like dislocations is not considered for the sake of simplicity. Coupling between diffusion and climb was explicitely investigated in the reference [18]. By definition, the material point velocity is the average velocity of the atoms in the material volume element, V, here expressed in the referential of the lattice as:

$$\underline{\boldsymbol{v}}(\underline{\boldsymbol{x}}, t) = \frac{1}{n^a V} \sum_{n=1}^{n^a V} \underline{\boldsymbol{v}}^{a,n}(\underline{\boldsymbol{x}}, t) \ , \tag{2.2}$$

where $\underline{\boldsymbol{v}}^{a,n}(\underline{\boldsymbol{x}},t)$ is the velocity of the nth atom in V, and $n^a\,V$ the number of moles of atoms in V. Similarly for the vacancies:

$$\underline{\boldsymbol{v}}^{v}(\underline{\boldsymbol{x}},t)=\frac{1}{n^{v}V}\sum_{n=1}^{n^{v}V}\underline{\boldsymbol{v}}^{v,n}(\underline{\boldsymbol{x}},t)\ . \tag{2.3}$$

Since the nth atom is either immobile ($\underline{\boldsymbol{v}}^{a,n}=0$) or exchanging position with the mth vacancy ($\underline{\boldsymbol{v}}^{a,n}=-\underline{\boldsymbol{v}}^{v,m}$),

$$\sum_{n=1}^{n^{a}V}\underline{\boldsymbol{v}}^{a,n}+\sum_{m=1}^{n^{v}V}\underline{\boldsymbol{v}}^{v,m}=0\ . \tag{2.4}$$

Using the network constraint, (2.1), and the definitions of the mean velocities given by (2.2) and (2.3), in (2.4), the following relation is obtained:

$$n^{a}\underline{\boldsymbol{v}}+n^{v}\underline{\boldsymbol{v}}^{v}=0\ . \tag{2.5}$$

The definition of the vacancy flux in $\mathrm{m}^{-2}\mathrm{s}^{-1}$ is defined as:

$${}^{n}\underline{\boldsymbol{j}}^{v}=n^{v}\underline{\boldsymbol{v}}^{v}\ , \tag{2.6}$$

where the left upperscript, n, reminds us that this definition is valid for molar concentrations. Substituting (2.6) into (2.5), a relation between the velocity of the atoms and the vacancy flux is obtained,

$$\underline{\boldsymbol{v}}=-\frac{1}{n^{a}}{}^{n}\underline{\boldsymbol{j}}^{v}\ . \tag{2.7}$$

The motion of the atoms described by (2.7) gives rise to a deformation rate, defined as the symmetric part of the velocity gradient. Then,

$$D_{ij}=\frac{1}{2}\left(\frac{\partial v_i}{\partial x_j}+\frac{\partial v_j}{\partial x_i}\right). \tag{2.8}$$

Using (2.7), the deformation rate can be finally related to the gradient of the vacancy flux, as,

$$D_{ij}=-\frac{1}{2}\left(\frac{\partial}{\partial x_j}\left(\frac{1}{n^{a}}{}^{n}j_i^{v}\right)+\frac{\partial}{\partial x_i}\left(\frac{1}{n^{a}}{}^{n}j_j^{v}\right)\right). \tag{2.9}$$

The equations (2.8) and (2.9), respectively, correspond to equations (1) and (2) in [2], where the same notion of a material point defined by a group of atoms was employed in a continuum mechanics based coupled stress-diffusion formulation. In that work, the simplifying assumption that vacancies are neither created nor annihilated was made. The equation (2.9) from the present work shows a direct link between the inelastic strain rate tensor and the vacancy flux gradient. It is believed that the atom/marker based definition of a material point used here is the best suited to compare computational results with strain field measurements based on fiducial grids in polycrystalline aggregates.

2.3. Balance of species

Consider the material domains, $\mathcal{D}$ and $\mathcal{D}_0$, as material subdomains of $\mathcal{B}$ and $\mathcal{B}_0$, respectively. In this section, it is assumed that the number of substitutional sites remains practically constant. Hence,

$$\int_{\mathcal{D}_0} N^{\#}(\underline{\boldsymbol{X}})\mathrm{d}V = \int_{\mathcal{D}} n^{\#}(\underline{\boldsymbol{x}},t)\mathrm{d}v \ . \tag{2.10}$$

Differentiating (2.10) with respect to time and using Reynold's transport equation yields,

$$0 = \frac{\partial}{\partial t}\int_{\mathcal{D}} n^{\#}(\underline{\boldsymbol{x}},t)\mathrm{d}v = \int_{\mathcal{D}}\left(\frac{\partial n^{\#}}{\partial t} + n^{\#}\frac{\partial v_i}{\partial x_i}\right)\mathrm{d}v \ , \tag{2.11}$$

which leads to the local form of the sites balance equation:

$$\frac{\partial n^{\#}}{\partial t} + n^{\#}\mathrm{div}\ \underline{\boldsymbol{v}} = 0 \ . \tag{2.12}$$

The balance law for vacancies, is then expressed in terms of c^v, the lattice site fraction of vacancies, as,

$$\begin{aligned}
\frac{\mathrm{d}}{\mathrm{d}t}\int_{\mathcal{D}} n^{\#}c^v\mathrm{d}v \qquad\qquad &= -\int_{\partial\mathcal{D}} {}^{n}\underline{\boldsymbol{j}}^v\cdot\underline{\boldsymbol{n}}, \\
\int_{\mathcal{D}} n^{\#}\dot{c}^v + c^v\left(\frac{\partial n^{\#}}{\partial t} + n^{\#}\mathrm{div}\ (\underline{\boldsymbol{v}})\right)\mathrm{d}v &= -\int_{\partial\mathcal{D}} {}^{n}\underline{\boldsymbol{j}}^v\cdot\underline{\boldsymbol{n}}, \\
\int_{\mathcal{D}} n^{\#}\dot{c}^v\mathrm{d}v \qquad\qquad &= -\int_{\partial\mathcal{D}} {}^{n}\underline{\boldsymbol{j}}^v\cdot\underline{\boldsymbol{n}} \ ,
\end{aligned} \tag{2.13}$$

where the Reynolds transport theorem and the conservation of sites, (2.12), has been used. Since $n^{\#}$ is practically constant, the local form of (2.14) can be divided by $n^{\#}$ to obtain new definitions in terms of c^v instead of n^v. Hence, a new definition of the vacancy flux having units of [m s^{-1}] will be henceforth used [25],

$$\underline{\boldsymbol{j}}^v = c^v\underline{\boldsymbol{v}}^v \ , \tag{2.14}$$

which satisfies the field equation,

$$\dot{c}^v = -\mathrm{div}\ (\underline{\boldsymbol{j}}^v) \ . \tag{2.15}$$

It is recalled that the balance equation (2.15) is valid for the bulk grain behaviour in the absence of sources and sinks, thus the interaction of vacancies with crystal defects is excluded for simplicity.

2.4. Linearized theory

It is here assumed that $c^v \ll 1$. The components of the strain rate equation, (2.9), is now expressed as:

$$D_{ij} = -\frac{1}{2}\left(\frac{\partial}{\partial x_j}\left(\frac{1}{(1-c^v)}j_i^v\right) + \frac{\partial}{\partial x_i}\left(\frac{1}{(1-c^v)}j_j^v\right)\right). \tag{2.16}$$

The linearized strain rate components are finally given by,

$$D_{ij} = -\frac{1}{2}\left(\frac{\partial j_i^v}{\partial x_j} + \frac{\partial j_j^v}{\partial x_i}\right). \tag{2.17}$$

The strain rate can be split into two parts, as follows,

$$\underset{\sim}{\boldsymbol{D}} = \frac{\text{trace}\,(\underset{\sim}{\boldsymbol{D}})}{3}\underset{\sim}{\mathbf{1}} + \underset{\sim}{\boldsymbol{D}}^{\text{dev}}\ . \tag{2.18}$$

The volumetric part corresponds to an accumulation or loss of vacancies and is associated with an eigenstrain proportional to the vacancy concentration, since $\text{trace}\,(\underset{\sim}{\boldsymbol{D}}) = -\text{div}\,\underline{\boldsymbol{j}}^v = \dot{c}^v = -\dot{c}^a$. The deviatoric part, $\underset{\sim}{\boldsymbol{D}}^{\text{dev}}$, can be defined as the inelastic creep strain rate. Its integrated form leads to the sheared deformation illustrated in figure 1. Finally, an elastic deformation can be superimposed on the previous contributions. Note that Berdichevsky [2] introduces elastic and plastic velocities. However, there is generally not such a thing like an elastic or plastic velocity, since elastic and plastic strain tensors are generally incompatible.

3. Balance laws and constitutive equations in elasto-viscoplasticity

3.1. Balance laws

The balance law for vacancies, (2.15), has already been derived on the volume $\mathcal{B}$ with boundary $\partial\mathcal{B}$ of normal $\underline{\boldsymbol{n}}$:

$$\begin{aligned} &\dot{c}^v = -\text{div}\,\underline{\boldsymbol{j}}^v + s^v \text{ on } \mathcal{B} \\ &j^v = \underline{\boldsymbol{j}}^v \cdot \underline{\boldsymbol{n}} \text{ on } \partial\mathcal{B} \end{aligned} \tag{3.1}$$

Note that a source/sink term s^v has been added to equation (2.15). This term is taken to be zero in the grain's interior, as already stated, but can be active in the grain boundary region, as explained in section 4.1. The mechanical static equilibrium in the absence of volume forces is governed by:

$$\begin{aligned} &\text{div}\,\underset{\sim}{\boldsymbol{\sigma}} = 0 \text{ on } \mathcal{B} \\ &\underline{\boldsymbol{t}} = \underset{\sim}{\boldsymbol{\sigma}} \cdot \underline{\boldsymbol{n}} \text{ on } \partial\mathcal{B} \end{aligned} \tag{3.2}$$

where $\underset{\sim}{\boldsymbol{\sigma}}$ is the stress tensor and $\underline{\boldsymbol{t}}$ the traction vector on $\partial\mathcal{B}$.

3.2. Constitutive equations

The small strain tensor, $\underset{\sim}{\boldsymbol{\varepsilon}}$, is partitioned into four contributions

$$\underset{\sim}{\boldsymbol{\varepsilon}} = \underset{\sim}{\boldsymbol{\varepsilon}}^e + \underset{\sim}{\boldsymbol{\varepsilon}}^\star(c^v) + \underset{\sim}{\boldsymbol{\varepsilon}}^{\text{in-diff}} + \underset{\sim}{\boldsymbol{\varepsilon}}^{\text{in-disl}}\ , \tag{3.3}$$

where

- $\underset{\sim}{\boldsymbol{\varepsilon}}^e$ is the elastic strain tensor,
- $\underset{\sim}{\boldsymbol{\varepsilon}}^\star(c^v)$ is the eigenstrain tensor due to the relaxation of the lattice around vacancies,
- $\underset{\sim}{\boldsymbol{\varepsilon}}^{\text{in-diff}}$ is the inelastic strain tensor due to inhomogeneous vacancy motion,
- $\underset{\sim}{\boldsymbol{\varepsilon}}^{\text{in-disl}}$ is the inelastic strain tensor due to dislocation motion.

The eigenstrain typically depends on the concentration, c^v, as [4]

$$\underset{\sim}{\boldsymbol{\varepsilon}}^\star(c^v) = \underset{\sim}{\boldsymbol{\eta}}^v(c^v - c^v_{\text{ref}}) + \underset{\sim}{\boldsymbol{\varepsilon}}^\star_{\text{ref}} \tag{3.4}$$

Here, $\underset{\sim}{\boldsymbol{\varepsilon}}^{\star}_{\mathrm{ref}}$ is the eigenstrain tensor corresponding to the equilibrium concentration, c^{v}_{ref}, and $\underset{\sim}{\boldsymbol{\eta}}^{v}$ defines the direction and magnitude of the surrounding atomic relaxation. The diffusion creep term, $\underset{\sim}{\boldsymbol{\varepsilon}}^{\mathrm{in-diff}}$, is the deviatoric part of (2.17)

$$\dot{\varepsilon}_{ij}^{\mathrm{in-diff}} = -\left(\frac{1}{2}\left(\frac{\partial j_i^v}{\partial x_j} + \frac{\partial j_j^v}{\partial x_i}\right) - \frac{1}{3}\frac{\partial j_k^v}{\partial x_k^v}\delta_{ij}\right). \tag{3.5}$$

Note that in previous work (e.g. [21, 26]), the diffusion-induced inelastic creep strain was accounted for using a power or exponential viscous flow rule, directly relating $\dot{\underset{\sim}{\boldsymbol{\varepsilon}}}^{\mathrm{in-diff}}$ to the deviatoric stress. In contrast, here, it is computed from the gradient of the diffusion flux. The inelastic strain rate tensor due to dislocation motion, $\dot{\underset{\sim}{\boldsymbol{\varepsilon}}}^{\mathrm{in-disl}}$, can be expressed using the crystal plasticity framework as,

$$\dot{\underset{\sim}{\boldsymbol{\varepsilon}}}^{\mathrm{in-disl}} = \sum_{\alpha} \frac{1}{2}\dot{\gamma}^{\alpha}(\underline{\boldsymbol{m}}^{\alpha} \otimes \underline{\boldsymbol{n}}^{\alpha} + \underline{\boldsymbol{n}}^{\alpha} \otimes \underline{\boldsymbol{m}}^{\alpha}) \,, \tag{3.6}$$

where the superscript, α, denotes the slip system, $\dot{\gamma}^{\alpha}$ the crystallographic slip rate, $\underline{\boldsymbol{n}}^{\alpha}$ the slip system plane normal, and $\underline{\boldsymbol{m}}^{\alpha}$ the slip direction. The kinetic equation for the crystallographic slip rate, $\dot{\gamma}^{\alpha}$, is expressed using a power law relation,

$$\dot{\gamma}^{\alpha} = \left\langle \frac{|\tau^{\alpha}| - S_T^{\alpha}}{\tau_0} \right\rangle^{n} \mathrm{sign}(\tau^{\alpha}) \,, \tag{3.7}$$

where, τ^{α}, is the resolved shear stress, τ_0 and n are material viscosity parameters, and S_T^{α} is the overall slip resistance. The latter is given by [21] :

$$S_T^{\alpha} = \lambda G b^{\alpha} \sqrt{\sum_{\beta} h_{\alpha\beta}\rho^{\beta}} \,, \tag{3.8}$$

in which, λ, is a coefficient, G the shear modulus, b^{α} the magnitude of the Burgers vector, ρ^{α} the overall dislocation density, and $h_{\alpha\beta}$ a dislocation interaction matrix expressed in terms of two coefficients, ω_1 and ω_2, as

$$h_{\alpha\beta} = \omega_1 + (1 - \omega_2)\delta_{\alpha\beta} \,. \tag{3.9}$$

Note that, for simplicity, no direct coupling of diffusion with dislocation multiplication and annihilation is introduced in this work. The power law expression, (3.7), indirectly accounts for vacancy diffusion mediated climb processes. A more direct coupling was recently proposed in [18] at a lower scale. A dependence of the diffusion coefficient on dislocation density could be introduced following, for instance, [27]. Finally, the evolutionary equation for the dislocation density reads [21]

$$\dot{\rho}^{\alpha} = \frac{C}{b^{\alpha}}\left[K\sum_{\beta}\rho^{\beta} - 2d_p\rho^{\alpha}\right]|\dot{\gamma}^{\alpha}| \,, \tag{3.10}$$

where C, K and d_p are material hardening parameters. The Helmholtz free energy density is assumed to be composed of a mechanical and a chemical part:

$$\psi(c^v, \underset{\sim}{\boldsymbol{\varepsilon}}^e) = \psi^{\mathrm{mech}}(\underset{\sim}{\boldsymbol{\varepsilon}}^e) + \psi^{\mathrm{chem}}(c^v) \,. \tag{3.11}$$

The mechanical part of the free energy is defined as,

$$\psi^{\text{mech}}(\underset{\sim}{\boldsymbol{\varepsilon}}^e) = \frac{1}{2}\underset{\sim}{\boldsymbol{\varepsilon}}^e : \underset{\approx}{\boldsymbol{\Lambda}} : \underset{\sim}{\boldsymbol{\varepsilon}}^e \ , \tag{3.12}$$

where, $\boldsymbol{\Lambda}$, is the fourth order elasticity tensor, taken independent of c^v for simplicity. The chemical free energy density is expressed in a standard form as [28],

$$\psi^{\text{chem}}(c^v) = \frac{E_f}{\Omega_0}c^v + \frac{RT}{\Omega_0}(c^v \log(c^v) + (1-c^v)\log(1-c^v)) \tag{32}$$

where, T, is the absolute temperature, R the ideal gas constant, E_f the vacancy formation energy, and Ω_0 the volume per mole of atoms. The state laws are given according to [29] :

$$\underset{\sim}{\boldsymbol{\sigma}} = \frac{\partial \psi}{\partial \underset{\sim}{\boldsymbol{\varepsilon}}^e} = \underset{\approx}{\boldsymbol{\Lambda}} : \underset{\sim}{\boldsymbol{\varepsilon}}^e \ , \tag{3.14}$$

$$\mu = \frac{\partial \psi}{\partial c^v} - \underset{\sim}{\boldsymbol{\eta}}^v : \underset{\sim}{\boldsymbol{\sigma}} \ , \tag{3.15}$$

where μ is the diffusion potential. The vacancy flux is defined as

$$\underline{\boldsymbol{j}}^v = -\underset{\sim}{\boldsymbol{L}}(c^v) \cdot \nabla \mu \ , \tag{3.16}$$

with the mobility, $\underset{\sim}{\boldsymbol{L}}^v$, expressed as

$$\underset{\sim}{\boldsymbol{L}}^v = \frac{\Omega_0}{RT}c^v(1-c^v)\underset{\sim}{\boldsymbol{D}}^v \ . \tag{3.17}$$

Here, $\underset{\sim}{\boldsymbol{D}}^v$, is the generally anisotropic diffusivity tensor [25].

4. Simulation of diffusional creep in a polycrystalline aggregates

4.1. Grain boundary description

The driving force for diffusion is the gradient of diffusion potential, defined by (3.15). According to Herring's theory, the inhomogeneity in the diffusion potential is introduced by the grain boundaries, and thus here they will be modeled explicitly. In 2D, the simplification is made that each grain can be described by a single orientation, θ, defined with respect to an arbitrary reference configuration [30]. A stationary phase-field, ϕ^{GB}, is introduced to interpolate physical properties between their bulk and grain boundary values. It is arbitrarily expressed as the following explicit function,

$$\phi^{\text{GB}}(d) = \left(\cosh\left(\frac{r^{\text{GB}} \times 2d}{\delta^{\text{GB}}}\right)\right)^{-1} \ , \tag{4.1}$$

where, δ^{GB}, is the grain diffuse boundary thickness and, d, the distance from any point to the closest grain boundary. Also, the coefficient $r^{\text{GB}} = 5.3$ is chosen so that $\phi^{\text{GB}}\left(\frac{-\delta^{\text{GB}}}{2}\right) = \phi^{\text{GB}}\left(\frac{\delta^{\text{GB}}}{2}\right) = 0.01$, thus defining the diffuse interface thickness. Furthermore, a second stationary phase-field function, θ, is relied upon in order to represent the grain

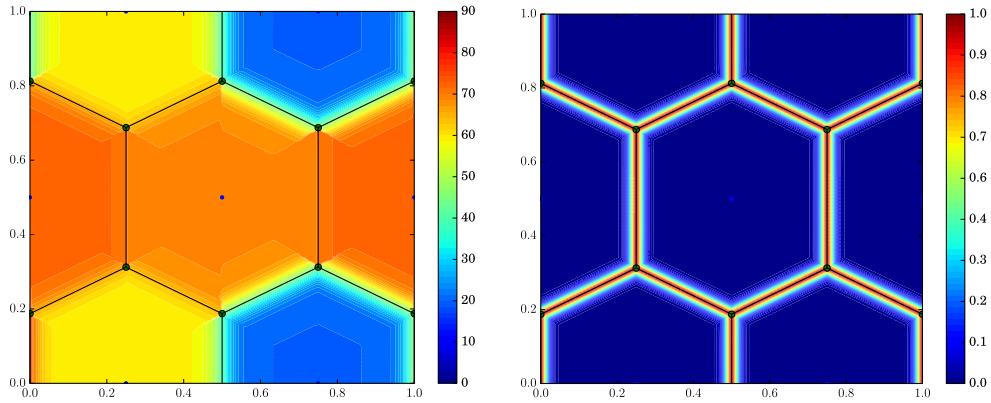

Figure 3. Periodic 2D polycrystal aggregate used in the simulations. The window size varies in the simulations from 20 to 200 μm. The edges of the Voronoi cells are superimposed to the fields. (a) Grain orientation field θ, generated randomly. (b) Grain boundary field ϕ^{GB}.

orientation to be used in the crystal plasticity model. This orientation field function varies smoothly between two grains of orientation θ_1 and θ_2, and is described by the following function,

$$\theta(\bar{d}) = \frac{1}{2}(\theta_1 - \theta_2)\left[1 - \tanh\left(-\frac{2.94\bar{d}}{\delta^{\mathrm{GB}}}\right)\right] + \theta_2 \ , \tag{4.2}$$

where, $\bar{d}$, is the algebraic distance to the grain boundary, negative in the grain oriented along θ_1 and positive in the grain with orientation θ_2, such that $\theta(0) = \frac{\theta_1+\theta_2}{2}$, $\theta\ (-\infty) = \theta_1$ and $\theta\ (+\infty) = \theta_2$. Both ϕ^{GB} and θ fields are shown in figure 3. Note that the interpolation equation (4.2) induces discontinuities in the θ field within the grains if more than two grains are considered. An equilibrium orientation field generated by a phase field type model, as done in [20, 31], would be preferable. We have verified that this choice (4.2) does not significantly affect the crystal plasticity results presented in section 4.3.3 by comparison with computations based on a uniform lattice orientation in each grain as done usually in standard crystal plasticity simulations.

The value of θ within each grain has been generated randomly. The diffusivity tensors are expressed as:

$$\begin{aligned} \underset{\sim}{\boldsymbol{D}}^{v} &= (1-\phi^{\mathrm{GB}})\underset{\sim}{\boldsymbol{D}}^{v}_{\mathrm{bulk}} + \phi^{\mathrm{GB}}\underset{\sim}{\boldsymbol{D}}^{v}_{\mathrm{GB}} \\ \underset{\sim}{\boldsymbol{D}}^{v}_{\mathrm{bulk}} &= D^{v}_{\mathrm{bulk}}\underset{\sim}{\boldsymbol{I}} \\ \underset{\sim}{\boldsymbol{D}}^{v}_{\mathrm{GB}} &= D^{v}_{\mathrm{GB}}(\underset{\sim}{\boldsymbol{I}} - \underline{\boldsymbol{n}} \otimes \underline{\boldsymbol{n}}) \end{aligned} \tag{4.3}$$

In the above relation, the grain boundary normal is computed numerically using $\underline{\boldsymbol{n}} = \frac{\underline{\nabla}\theta}{\|\underline{\nabla}\theta\|}$. Furthermore, the parameter $\underset{\sim}{\boldsymbol{\eta}}^{v}$ is chosen such that the Herring diffusion potential formula is recovered,

$$\underset{\sim}{\boldsymbol{\eta}}^{v} = (1-\phi^{\mathrm{GB}})\eta^{v,\mathrm{bulk}}\underset{\sim}{\boldsymbol{I}} + \phi^{\mathrm{GB}}\eta^{v,\mathrm{GB}}\underline{\boldsymbol{n}} \otimes \underline{\boldsymbol{n}} \ . \tag{4.4}$$

The coefficients $\eta^{v,\text{bulk}}$ and $\eta^{v,\text{GB}}$ are expressed as:

$$\eta^{v,\text{bulk}} = \frac{\Delta v^{v,\text{bulk}}}{3\Omega_0}\,, \eta^{v,\text{GB}} = \frac{\Delta v^{v,\text{GB}}}{3\Omega_0}\,, \tag{4.5}$$

where, $\Delta v^{v,\text{bulk}}$ and $\Delta v^{v,\text{GB}}$ are, respectively, the bulk and grain boundary relaxed volume around a vacancy, and Ω_0 is the atomic volume. With this definition, the diffusion potential, (3.15), becomes:

$$\mu^v = \frac{E_f}{\Omega_0} + \frac{RT}{\Omega_0}\log\left(\frac{c^v}{1-c^v}\right) - \eta^{v,\text{bulk}}\text{trace}\,(\underset{\sim}{\boldsymbol{\sigma}})(1-\phi^{\text{GB}}) \; - \eta^{v,\text{GB}}\sigma_n\phi^{\text{GB}}\,, \tag{4.6}$$

where, $\sigma_n = \underset{\sim}{\boldsymbol{\sigma}} : \underline{\boldsymbol{n}} \otimes \underline{\boldsymbol{n}}$ is the normal GB traction. The above expression for the diffusion potential, μ^v, can be compared to the formula derived by Herring in [1]:

$$\mu - \mu_h = \mu_0 - p_{zz}\Omega_0\,, \tag{4.7}$$

where $(\mu - \mu_h)$ is the diffusion potential, μ_0 is defined by Herring as '*the chemical potential of […] the same substance in equilibrium at the same temperature and at zero stress*', p_{zz} the normal surface traction, and $\Omega_0 = \frac{\delta v}{\delta N}$ the atomic volume corresponding to the addition/removal of δN atoms causing a change in volume, δv. Albeit the physical unit difference (Herring used a flux in atoms per unit area per unit time), one can observe that the diffusion potential derived in (4.6) contains the same terms. Using (3.15), the gradient of the diffusion potential becomes:

$$\underline{\nabla}\mu^v = \frac{\partial^2\psi}{\partial c^2}\nabla c \; + \left(-\frac{\partial \underset{\sim}{\boldsymbol{\eta}}^v}{\partial\phi^{\text{GB}}} : \underset{\sim}{\boldsymbol{\sigma}} + \frac{\partial^2\psi}{\partial c\partial\phi^{\text{GB}}}\right)\nabla\phi^{\text{GB}} + \left(-\frac{\partial^2\psi}{\partial\underset{\sim}{\boldsymbol{\varepsilon}}^e\partial\underset{\sim}{\boldsymbol{\varepsilon}}^e} : \underset{\sim}{\boldsymbol{\eta}}^v\right) : \nabla\underset{\sim}{\boldsymbol{\varepsilon}}\,, \tag{4.8}$$

and it is readily seen that any mechanical loading of the grain boundaries will give a non-zero diffusion potential gradient, leading in turn to a creep deformation via (2.17).

It is commonly accepted that grain boundaries, and interfaces in general, act as sources and sinks for point defects [19, 32, 33]. Grain boundaries are also known to interact with dislocations [34, 35], but this coupling is not taken into account in the present work. In what follows, two modelling options will be explored. First, a Dirichlet boundary condition imposing the equilibrium concentration of vacancies in the grain boundary region will be used, as done in [8]. Second, an additional source term in the diffusion equation (2.15) needs to be defined such that the grain boundary vacancy concentration is always close to its equilibrium value, as per [5, 36]. Then,

$$\dot{c}^v = -\text{div}\,\underline{\boldsymbol{j}}^v - K_{\text{sv}}^{\text{GB}}(c^v - c_{\text{eq}}^{v,\text{GB}})\phi^{\text{GB}} \quad \text{on } V\,, \tag{4.9}$$

$$j^v = \underline{\boldsymbol{j}}^v \cdot \underline{\boldsymbol{n}} \quad \text{on } \partial V\,. \tag{4.10}$$

Even though conservation of lattice sites has been assumed in the bulk material, this does not hold in the grain boundary regions, which act as preferential location for vacancy creation and annihilation [32]. It is supposed that the site creation/destruction rate, $\dot{n}^{\#}$, see equation (2.11), is related to the vacancy source term, ${}^{n}s^v$, as illustrated in figure 4.

As an example, first consider the case of a grain boundary acting as a sink for vacancies. Vacancies that migrate toward this grain boundary will eventually reach the last lattice sites located on the grain boundary surface itself. In a random grain boundary region, this row of lattice sites simply vanishes, thus producing a deformation at this grain boundary. Second, the exact inverse process happens at grain boundaries acting as sources: atoms at the surface will

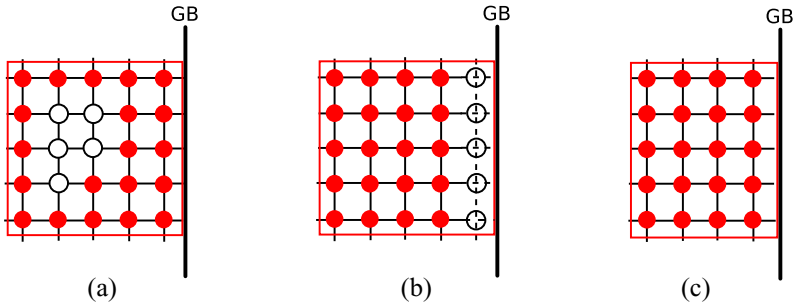

Figure 4. Mechanism for vacancy diffusion creep in a grain boundary region: (a) vacancies diffuse in the grain boundary vicinity, (b) when they reach the grain boundary surface, they destroy lattice sites, and (c) the grain boundary region shrinks as a result.

create a hump and leave a vacancy in the sites that they previously occupied. This process is repeated until a whole new row of lattice sites is created. Hence, matter is transported from the GB that acts as a vacancy source, and which thickens in the process, toward the one acting as a sink, which shrinks. In [10] section 7.1, Mishin and co-workers comments their model, stating that '*Vacancies can be generated only within the GB region and only by the growth or dissolution of lattice planes parallel to the GB*'. Due to the fact that the molar quantity being absorbed or emitted by the grain boundary is known from (4.9), it is possible to take into account this additional phenomenon by completing the creep rate (3.5) in the grain boundary region, to distinguish between bulk processes and grain boundary processes, as:

$$\dot{\varepsilon}_{ij}^{in-diff} = -\left(\frac{1}{2}\left(\frac{\partial j_i^v}{\partial x_j} + \frac{\partial j_j^v}{\partial x_i}\right) - \frac{1}{3}\frac{\partial j_k^v}{\partial x_k^v}\delta_{ij}\right)(1-\phi^{\mathrm{GB}}) + \eta^{v,\mathrm{GB}}K_{\mathrm{sv}}(c^v - c_{\mathrm{eq}}^v)\phi^{\mathrm{GB}}n_i n_j \ . \tag{4.11}$$

In [5], the same boundary process has been proposed and derived. However, as emphasised by the authors, this leads to creep strain accumulation only in the grain boundary regions. In the present work, viscoplastic strain is also introduced in the bulk part of the grain.

Grain boundary sliding and opening are additional important deformation modes when considering creep deformation and damage. However, they are not incorporated in the presented simulations for the sake of simplicity. They can be added in the finite element simulations using the theoretical and computational methodologies such as those described in the references [37–39]. However, these processes involve strongly non-linear local material responses and lead to high computational costs.

4.2. Problem description

To illustrate the proposed theory, a simplified copper polycrystal made up of periodic 2D hexagonal grains is constructed, see figure 3. Creep simulations are conducted at 830 K, and compared with experimental data from [23, 40], and to the well known analytical solution for Herring-Nabarro creep [19], namely

$$\dot{\varepsilon} = \frac{BD^v c^v \sigma^L \Omega_0}{d_g^2 kT} \ , \tag{4.12}$$

where, d_g, is the grain size, B, a geometrical factor (here taken equal to 2), σ^L, the applied stress, and k the Boltzmann constant.

Table 1. Material parameters for copper.

C_{11} [GPa]	C_{12} [GPa]	C_{44} [GPa]	T_m [K]	D_0^v [m^2.s^{-1}]
179.5	126.4	82.5	1360.	3.4×10^{-5}
Q_a^v [J.mol^{-1}]	E_f^v [J.mol^{-1}]	$\eta^{v,\mathrm{GB}}$	$\eta^{v,\mathrm{bulk}}$	
2.0×10^5	1.225×10^5	-0.05	0	

Note: The properties are supposed to be the same in the grain boundaries as in the bulk for simplicity, except for the coefficient η^v, see (4.4).

Table 2. Parameters of the crystal plasticity model for pure copper.

τ_0 [MPa]	n	λ [21]	G [MPa] [21]	b^α [nm] [21]	$\rho^\alpha_{i=0}$ [μ m^{-2}]
200	4	0.3	45 000	0.257	3.2×10^4
ω_1 [21]	ω_2 [21]	C [21]	K [21]	d_p [μm] [21]	
1.5	1.2	0.5	1.4135×10^{-2}	10^{-3}	

The material parameters for copper are given in tables 1 and 2. The self-diffusion coefficient is expressed classically as $D = D^v c^v = D_0^v \exp\left(-\frac{Q_a^v}{RT}\right)$. An equi-axial stress $\boldsymbol{\sigma} = \sigma^L(\underline{\boldsymbol{e}}_y \otimes \underline{\boldsymbol{e}}_y - \underline{\boldsymbol{e}}_x \otimes \underline{\boldsymbol{e}}_x)$ is applied, of magnitudes ranging from 1 to 160 MPa, and for Ĩ0–100 μm grain sizes. The model is implemented into the finite element method, using the methodology described in [41 and 29]. The numerical implementation was carried out in the Z-set code [41], using a Newton resolution implicit scheme of the balance equations and a fourth order Runge-Kutta method with automatic time-stepping for the time integration of constitutive equations. In the calculation of the diffusion potential gradient, (4.8), the gradient of the total strain tensor is needed. Therefore, the total strain is interpolated from the Gauss points to the nodes using the shape functions, and its gradient computed via the derivatives of the shape functions. The same technique is used to compute the gradient of the vacancy flux vector. It should be noted that this method is identical to the one used by Thomas and Chopin [42], Abrivard *et al* [20], and Villani *et al* [29].

4.3. Results

Three cases are presented, where the proposed deformation mechanisms are progressively incorporated in the simulations. Two different boundary conditions in the GB region, either Dirichlet or K_{sv} sink term, are used. The GB is hence modelled as a perfect or potentially imperfect sink, respectively. While the Dirichlet condition is straightforward to use, the sink term formulation offers more flexibility in the modelling, provided the sink parameter K_{sv} is carefully chosen.

In the first case, Dirichlet boundary conditions are used, and the only viscoplastic contribution is the inelastic diffusional one, (3.5). In the second case, grain boundary deformation is accounted for, by mean of the constitutive equation, (4.11), and the extended vacancy balance law, (4.10). Finally, the two inelastic deformation mechanisms, (3.5) and (3.6), are taken into account in order to compare the numerical predictions with experimental data available in [23] for pure copper. Dirichlet boundary conditions are used in this last case.

All simulations have been carried out on the same polycrystalline aggregate, see figure 3. Periodic boundary conditions are imposed on the vacancy concentration field c^v, and the four external surfaces are constrained to remain flat. In all plots, the x and y coordinates are given in μm.

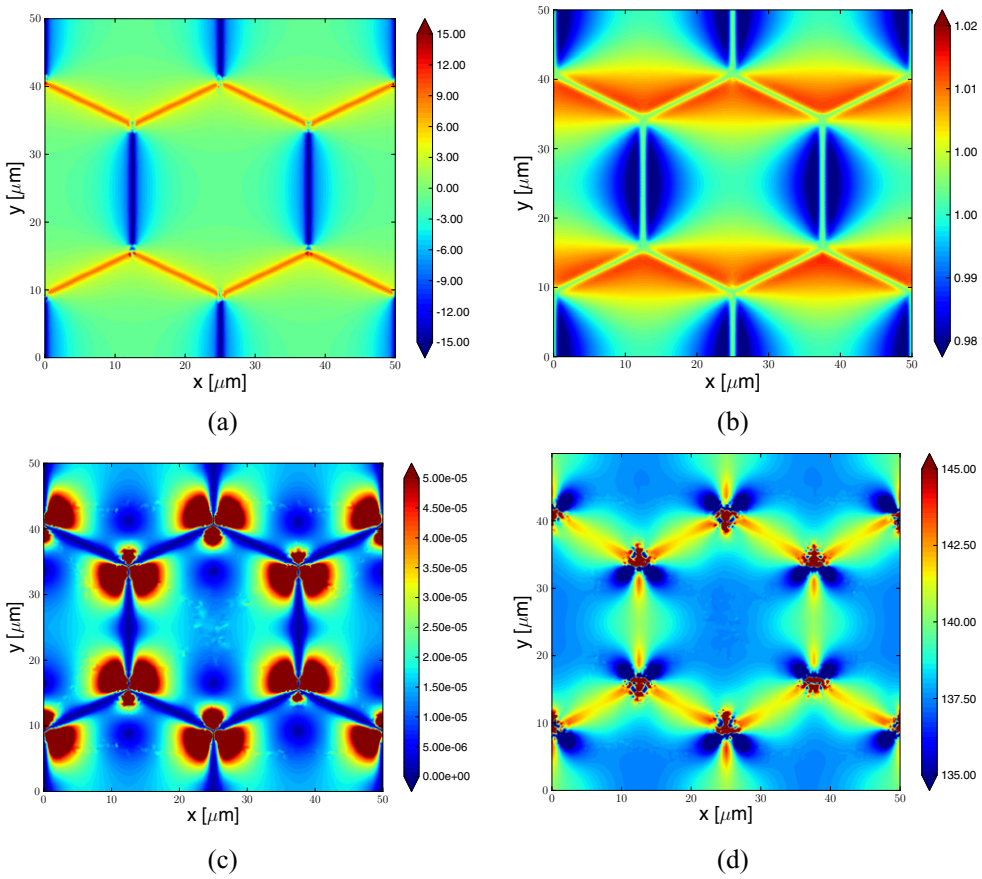

Figure 5. (a) Diffusion potential, (b) vacancy distribution, (c) inelastic strain and (d) equivalent Mises stress in the case of Dirichlet boundary conditions, with an applied stress of 80 MPa and a 25 μm grain size, and for isotropic elasticity. The mechanical effect on the diffusion potential is clearly visible in (a): the location of each grain boundary is revealed by a different diffusion potential value, depending on the GB orientation. (a) Diffusion potential μ immediately after the application of the stress. (b) Vacancy distribution normalised by c^v_{eq} at steady state. (c) Equivalent diffusional inelastic strain ($t = 5 \times 10^3$ s). (d) Equivalent Mises stress in MPa ($t = 5 \times 10^3$ s).

4.3.1. Case study one: Dirichlet conditions at the grain boundaries. In this case, $c^v = c^v{}_{\text{eq}}$ is imposed on the FE node lines corresponding to the grain boundaries, where $\phi^{\text{GB}} = 1$. In (4.11), K_{sv} is taken to be equal to 0 and, except for $\underset{\sim}{\boldsymbol{\eta}}$, the bulk and grain boundary properties are chosen to be the same in this section. For this first case, a first simulation is performed using isotropic elasticity: the symmetry in the geometry is visible in the resulting fields shown in figure 5. When the stress is applied, the diffusion potential value is modified depending on the grain boundary orientation. It reaches an extremum when the GB surface normal is parallel to one of the principal stress directions, according to (3.15), see figure 5(a). The equivalent inelastic strain, defined as $\varepsilon^{\text{in-diff}}_{\text{eq}} = \sqrt{\frac{2}{3}\underset{\sim}{\boldsymbol{\varepsilon}}^{\text{in-diff}} : \underset{\sim}{\boldsymbol{\varepsilon}}^{\text{in-diff}}}$, is shown on figure 5(c). Stress concentration effects are observed close to the grain boundary triple junctions in the case of elastic isotropy. Elastic anisotropy, shown in figure 6, leads to stronger heterogeneities, greater

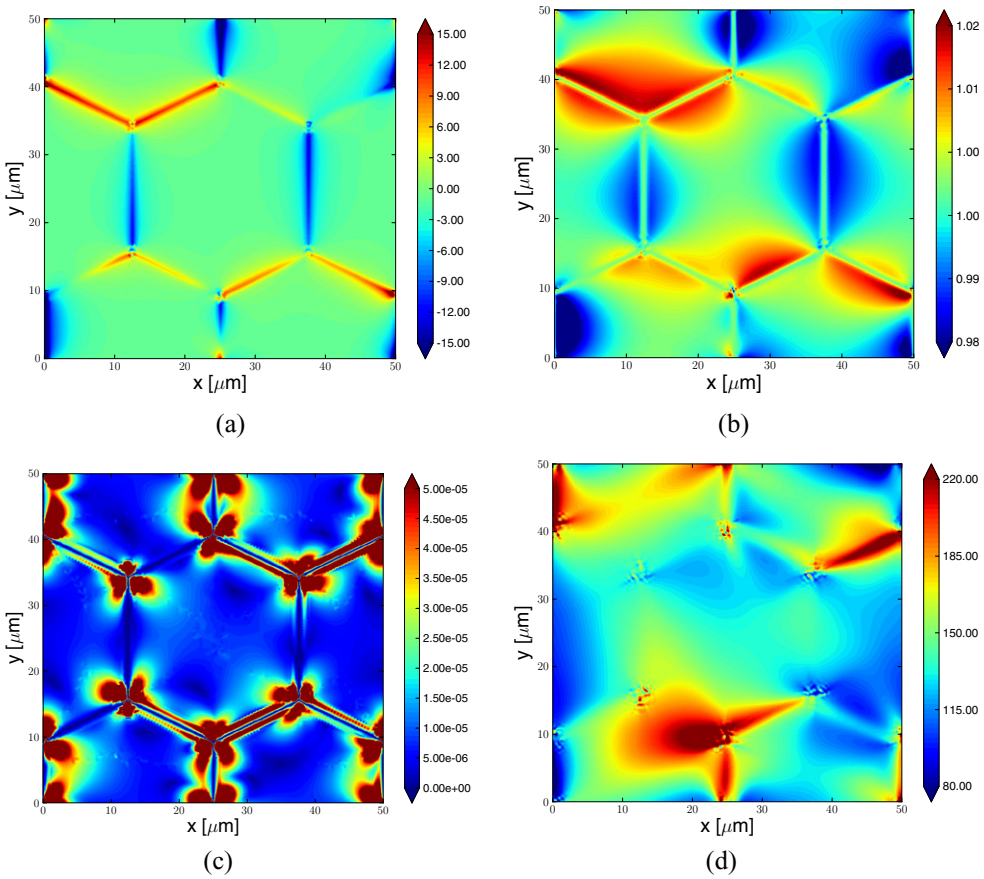

Figure 6. (a) Diffusion potential, (b) vacancy distribution, (c) inelastic strain and (d) equivalent Mises stress in the case of Dirichlet boundary conditions, with an applied stress of 80 MPa and a 25 μm grain size, and for anisotropic elasticity. (a) Diffusion potential μ immediately after the application of the stress. (b) Vacancy distribution normalised by c^v_{eq} at steady state. (c) Equivalent diffusional inelastic strain ($t = 5 \times 10^3$ s). (d) Equivalent Mises stress in MPa ($t = 5 \times 10^3$ s).

values of peak stresses, and breaks the hexagonal symmetry observed in the isotropic case. The strong stress and strain concentrations occuring at the triple junctions are due to increasing strain incompatibilities. Stress concentration regions lead generally to numerical convergence problems. Introduction of grain boundary sliding and opening, not done in the present modelling approach, would relax such stresses. Triple junctions are known to be responsible for cavity nucleation and subsequent damage, see [19].

The average macroscopic strain rate versus stress, and versus grain size on the other hand, are reported on figures 8(a) and (b), respectively. The model correctly predicts the strain rate scaling with respect to stress and grain size, i.e. $\dot{\varepsilon} = f(\sigma, d_g^{-2})$, and the overall strain rate is of the same order of magnitude as the one given by the analytical expression, (4.12). In order for the simulations to coincide with the analytical solution, the vacancy diffusivity coefficient has to be scaled up by a factor 7, which seems reasonable, since it is well within the experimental uncertainty. Finally, it should be pointed out that the simulations were carried out using two

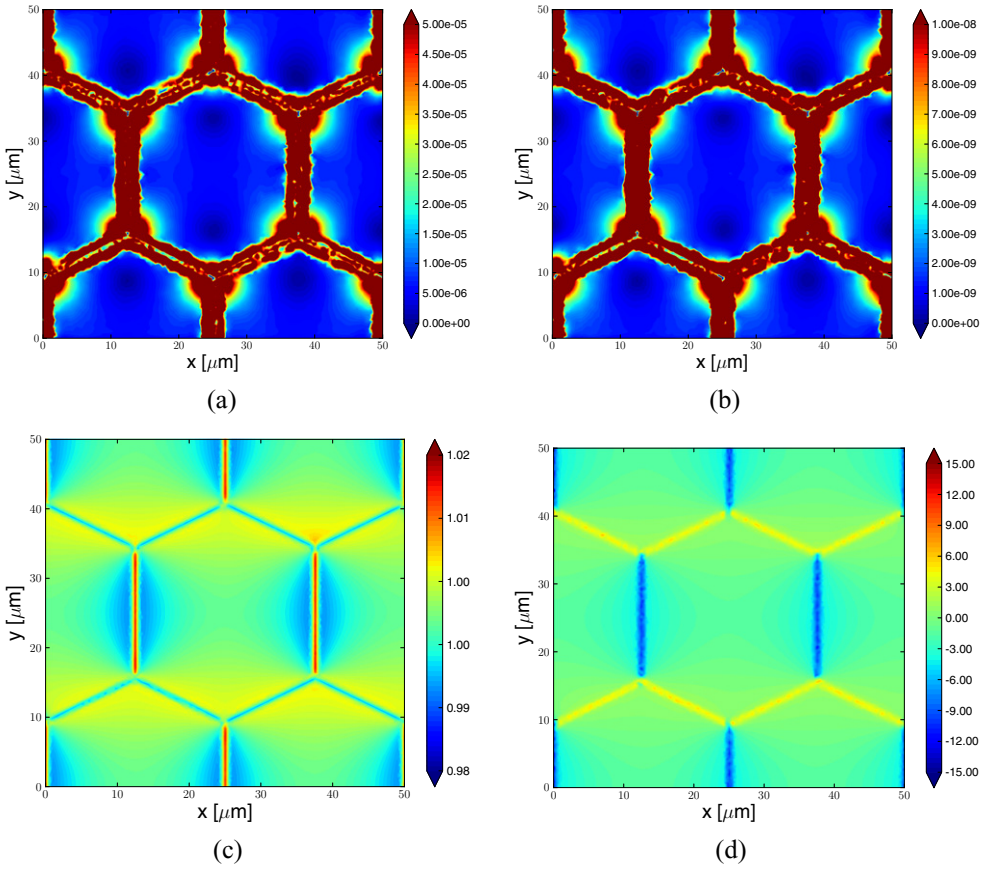

Figure 7. (a) Inelastic equivalent strain, (b) inelastic equivalent strain rate, (c) vacancy distribution and (d) diffusion potential μ in the case of a source term at the grain boundary, with an applied stress of 80 MPa and a 25 μm grain size, and for isotropic elasticity. (a) Equivalent diffusional inelastic strain ($t = 5 \times 10^3$ s). (b) Equivalent diffusional inelastic strain rate at steady state. (c) Vacancy distribution normalised by c^v_{eq} at steady state. (d) Diffusion potential $\mu(t = 5 \times 10^3$ s).

different meshes, one with 10 000 quadrangular quadratic elements, and the other with 98 000 triangular linear elements. No significant mesh sensitivity was found in the results.

4.3.2. Case study two: Source term in the grain boundaries. In this case, the Dirichlet boundary condition is dropped, and instead, the source strength parameter K_{sv} in (4.9) is set to a non-zero value and isotropic elasticity is used. In order to determine K_{sv}, a 1D case of two grains separated by a grain boundary is studied. First, a Dirichlet boundary condition on the grain boundary FE nodes is applied, as in the previous case. Then, the same problem is solved again, removing the Dirichlet condition and setting K_{sv} to be non zero at the grain boundary. The parameter K_{sv} is then chosen such that the concentration profiles given by both approaches are matched. For the range of grain sizes considered in this work, K_{sv} was found to be of the order of twice the vacancy diffusivity, $D^{v,\text{bulk}}$.

The grain boundary thickness, δ^{GB}, was kept constant and equal to 4 μm across the range of simulated grain sizes, and the mesh was constructed in such a way that there were always

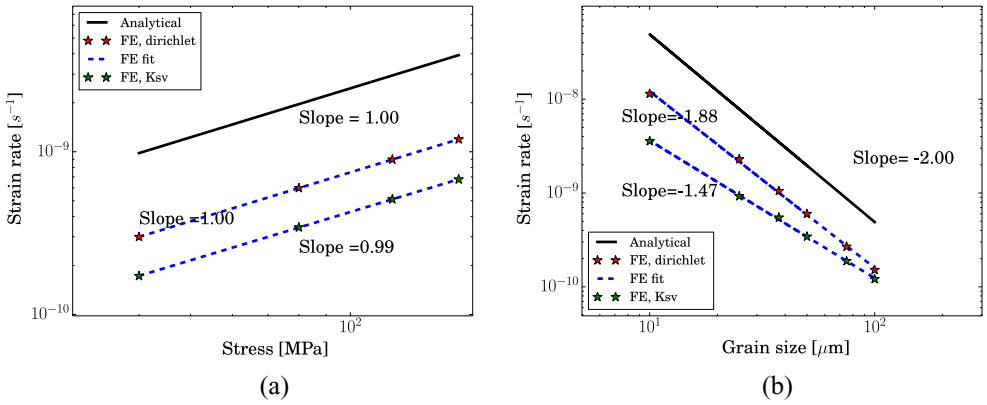

Figure 8. Comparison between the macroscopic Herring-Nabarro creep law and finite element simulations results using Dirichlet boundary conditions and sink term. According to the analytical solution, (4.12), the slopes in figures (a) and (b) should be 1 and −2, respectively. (a) Strain rate dependence on stress. (b) Strain rate dependence on grain size.

at least 5 elements in the grain boundary region. The grain boundary thickness was chosen as a compromise between reality (a dozen Burgers vectors) and tractable computations. The grain boundary volume fraction was hence taken to vary between 0.2 and 2.2×10^{-2} for the considered range of grain sizes.

The simulated fields are shown in figure 7 for the case of a 25 μm grain size and a 80 MPa applied stress. One can notice that in figure 7(a) deformation also accumulates in the grain boundary regions, minimizing the triple junction effect. Furthermore, despite the fact that the parameter K_{sv} was fitted with a 1D case, the steady state vacancy concentration in the grain boundary region in figure 7(c) is not exactly equal to c^v_{eq}. Instead, grain boundaries with $\sigma_n > 0$ have a lower vacancy concentration, and those with $\sigma_n < 0$, a higher one. However, the strain rate dependence on grain size is more strongly impacted when a source term is considered in the grain boundary, as it can be seen from figure 8(b).

4.3.3. Case study three: Dirichlet conditions at the grain boundary and crystal plasticity. In this last case, both inelastic deformations arising from vacancies diffusion, (3.5), and dislocation slip, (3.6), are taken into account. Dirichlet boundary conditions are used on the grain boundary nodes, and a value of $K_{sv} = 0$ is assumed. Anisotropic elasticity is used, and the parameters of the crystal plasticity model are given in table 2 for copper. Some are taken from the literature, as indicated in the table, and the other ones have been chosen so that the transition between the dislocation and diffusion regimes matches the experimental results presented in [23]. Hence, here the imposed stress is made to vary between 1 and 20 MPa.

The resulting strain and strain rate fields are shown on figure 9 for the 20 MPa case. Here, the dislocation regime is predominant, and the diffusional inelastic strain is strongly impacted by the slip activity. There are several differences to be observed between the purely diffusional case (figure 5) and the coupled case (figure 9), while bearing in mind that the stress level is different. Even though the vacancy distribution is similar, the maximum values are greater when crystal plasticity is considered. The same trend is observed for the diffusional field: the overall field is similar, but the strain rate is accelerated by dislocation induced plasticity despite the fact that the applied stress is four times smaller. Indeed, the inhomogeneities in the stress field arising from dislocation plasticity promote diffusion, and hence, diffusional creep.

Stress concentration is observed at some grain boundaries in figure 9(f), which is known from results of crystal plasticity finite element simulations [15].

Finally, the strain rate dependence on the applied stress is reported in figure 10. There are two visible regimes in this figure. At lower stress, diffusional deformation mechanisms dominate over slip activity, whereas the latter dominates for high applied stresses. This is in relatively good agreement with [23], albeit the value of the slope in the dislocation regime, which is greater in the simulations.

4.3.4. Discussion. The model predicts one order of magnitude lower strain rate in the diffusion regime, which can be explained by the fact that at low homologous temperature ($\simeq 0.6\ T_m$), grain boundary diffusion plays an important role. The grain boundary and bulk diffusion coefficients were assumed equal in the simulations, which is not necessarily the case in fcc materials. This may explain the lower average strain rate obtained numerically, compared to experimental data.

The value of the sink parameter, K_{sv}, was found to strongly influence the strain rate as well as the strain rate sensitivity to grain size. The value of this parameter, although critical, is not given in [5] (where it is actually called $\frac{1}{\tau}$). In this work, the sink parameter, K_{sv}, has been fitted from the results of a 1D simulation using Dirichlet boundary conditions. This approach, although very sensitive to the value of this parameter K_{sv}, is also capable of describing Herring-Nabarro creep. Furthermore, if one were to extend the proposed formalism to include migrating grain boundaries or void nucleation and growth, using for instance a phase-field approach [10, 36], the Dirichlet formulation would not be applicable. Indeed, some nodes that were once in a grain boundary region could, after grain boundary migration, be located in the bulk. In addition, voids, where $c^v = 1$, would be impossible to model, since a Dirichlet boundary condition would impose $c^v = c^v_{\mathrm{eq}} \ll 1$.

As pointed out above, the parameter K_{sv} has a significant influence on the strain rate and on the strain rate dependence on grain size, as shown in figure 8(b). Keeping the grain boundary width fixed, for an increasing value of K_{sv}, the overall strain rate increases since the contribution of the grain boundary increases as per (4.11), but the log(grain size)-log(strain rate) slope decreases. In contrast, for a decreasing K_{sv}, so does the macroscopic overall strain rate, but the slope increases.

Finally, the grain boundary width was reduced to 2 μm, as the GB region is expected to be of notable influence on the mechanical behavior [35]. Note that, in order to obtain realistic results, K_{sv} had to be multiplied by a factor ten compared to the 4 μm case. The dependence on the grain size is shown on figure 11, for the case of a 2 μm grain boundary width.

In the Case Study 3, a slip rate exponent, $n = 4$ in equation (3.7), was used, as it is a reasonable value for dislocation creep and close to that of 4.5 found experimentally in [23]. When there is no hardening, no slip threshold and no diffusion creep, the macroscopic response of the simulated polycrystal exhibits a slope of 4. In the present case, as a consequence of work hardening, the global response is more complex and different apparent exponent values are obtained, as it is well known when modelling creep in metals [41, 43].

5. Conclusions

A framework to model diffusion creep in polycrystals has been proposed, where individual grains and grain boundaries are explicitly modelled. It has been pointed out that, in the presence of diffusion, the material point definition should be handled with care, as material lines

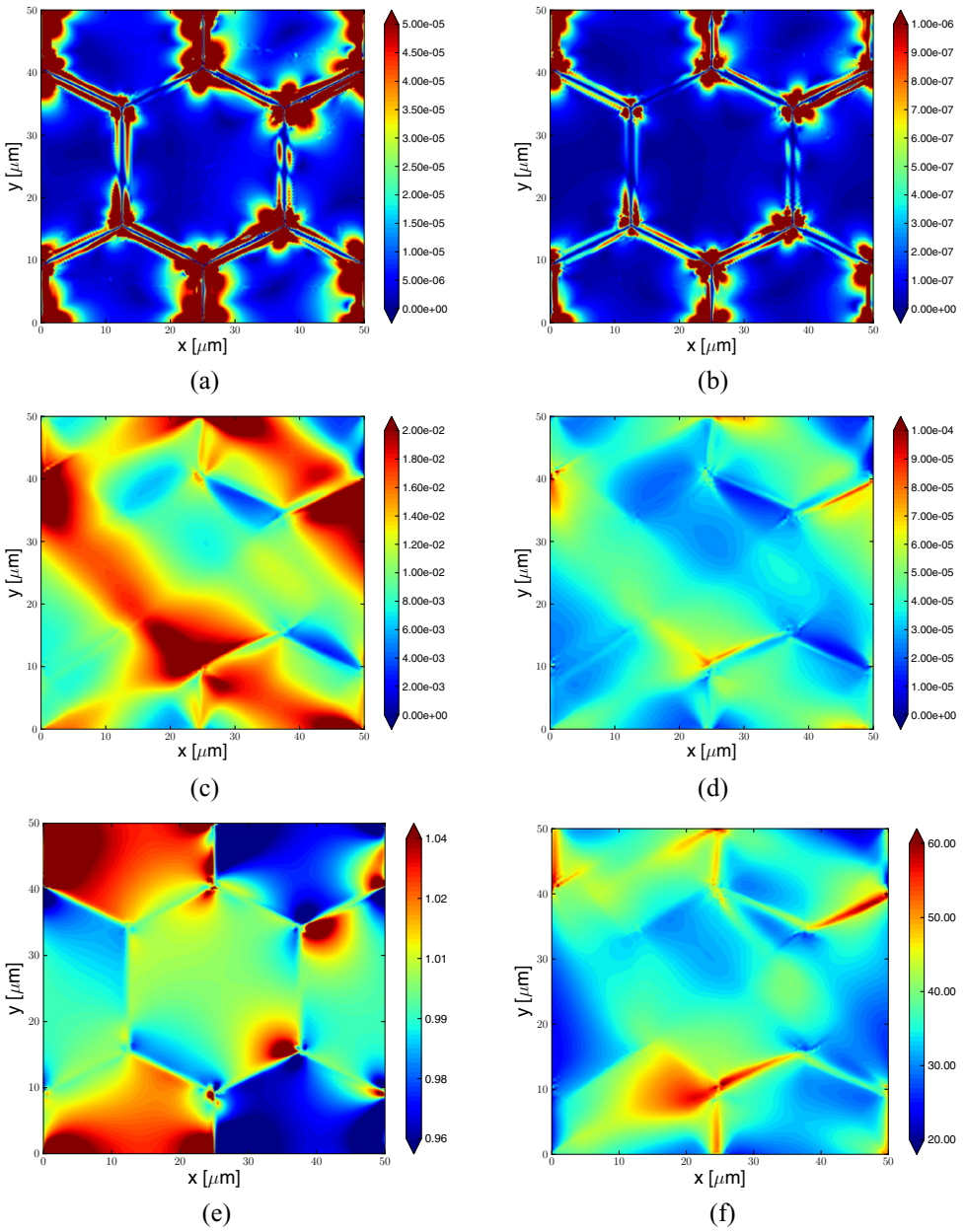

Figure 9. Inelastic (a) diffusional strain, (b) diffusional strain-rate, (c) dislocation strain, and (d) dislocation strain-rate, and (e) vacancy concentration and (f) equivalent Mises stress (applied stress of 20 MPa, 25 μm grain size and at $t = 10^3$ s). (a) Equivalent diffusional inelastic strain. (b) Equivalent diffusional inelastic strain rate. (c) Equivalent dislocation inelastic strain. (d) Equivalent dislocation inelastic strain rate. (e) Vacancy concentration normalised by c^v_{eq}. (f) Equivalent Mises stress in MPa.

drawn on the solid become blurred as diffusion occurs. Nevertheless, it is still possible to define and quantify a strain field in such cases, as long as moderate diffusion and relatively small concentration of vacancies are considered. It has been demonstrated that:

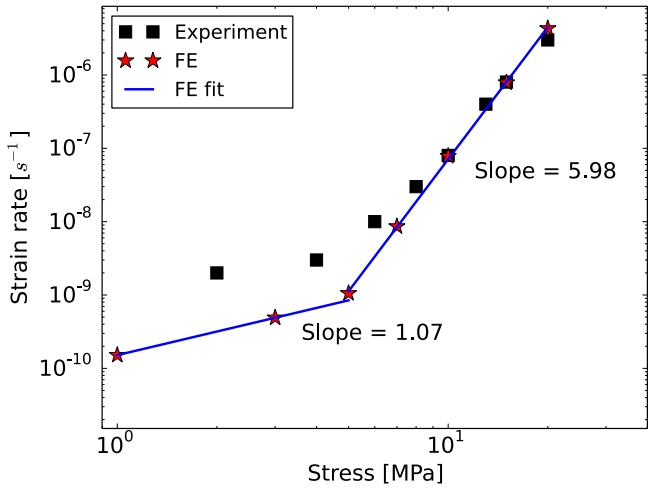

Figure 10. Strain rate dependence on stress. Data taken from [23].

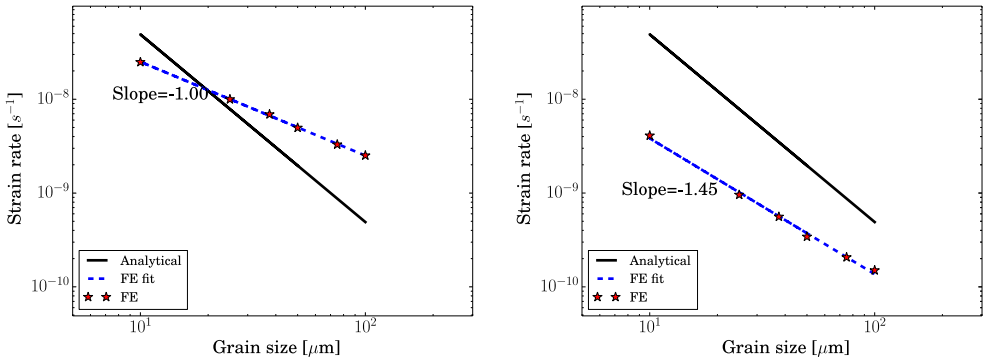

Figure 11. Comparison between the macroscopic Herring-Nabarro creep law and the finite element simulations results using a source term in the grain boundary of width 2 μm. According to (4.12), the slopes predicted analytically have a value of -2. (a) Strain rate dependence on grain size. (b) Strain rate dependence on grain size, ignoring grain boundary deformation process.

- Simple considerations of atom and vacancy motion have led to the definition of an inelastic diffusional strain rate on a perfect lattice, which has been related to the gradient of the vacancy flux.
- In order to retrieve the well known Herring diffusion potential formula, one has to define an anisotropic eigenstrain within the grain boundary regions, related to the normal of the grain boundary surface. Hence, any mechanical loading applied to the polycrystal directly induces vacancy motion, which, in turn, leads to creep strain.

The proposed diffusion induced deformation mechanism has been enriched by a classical crystal plasticity constitutive framework to account for the effects of dislocation creep. The framework has been implemented in a finite element model, with a detailed description of grain boundaries geometry and properties. The simulations that have been carried out show that:

- Strong heterogeneities are obtained at the intragranular level, especially at triple junctions.
- Anisotropic elasticity and dislocation induced plasticity promote the diffusion of vacancies and lead to higher diffusional strain rates, by developing stress gradients in the polycrystal.
- Classical macroscopic strain rate dependence on stress and grain size, that is $\dot{\varepsilon} = f(\sigma, d_g^{-2})$, are obtained, when using Dirichlet boundary conditions in the GB region. The use of a sink term also leads to a consistent macroscopic trend.
- The model predicts a smooth transition from diffusion dominated to dislocation dominated regime, depending on the applied stress level, as observed experimentally for copper [23].

Direct coupling between vacancy diffusion and dislocation climb was recently introduced in [18]. The continuum model presented therein could be complemented by the effect of the vacancy flux gradient in a straightforward manner. The proposed modelling framework is capable of reproducing Coble creep by properly choosing the diffusion parameters in the bulk and in the grain boundary regions. Furthermore, grain boundary sliding and damage are necessary mechanisms to be added to the present model to obtain a realistic description of creep mechanisms at the continuum polycrystalline level. The complete approach, incorporating the competing mechanisms of bulk and grain boundary diffusion, remains a challenging task and should be the objective of future work.

Acknowledgments

We are grateful to Dr Benoît Appolaire from ONERA, France, Prof M Geers from the Technische Universiteit Eindhoven, the Netherlands, Prof S Mesarovic from Washington State University and Mr V De Rancourt from the Ecole des Mines de Paris for fruitful discussions. Financial support by the European Commission through the project RadInterfaces (contract 10522) is gratefully acknowledged.

References

[1] Conyers Herring 1950 Diffusional viscosity of a polycrystalline solid *J. Appl. Phys.* **21** 437–45
[2] Berdichevsky V, Hazzledine P and Shoykhet B 1997 Micromechanics of diffusional creep *Int. J. Eng. Sci.* **35** 1003–32
[3] Suo Z 2004 A continuum theory that couples creep and self-diffusion *J. Appl. Mech.* **71** 646–51
[4] Cahn J W and Larché F 1985 The interactions of composition and stress in crystalline solids *Acta Metall.* **33** 331–57
[5] Garikipati K, Bassman L and Deal M 2001 A lattice-based micromechanical continuum formulation for stress-driven mass transport in polycrystalline solids *J. Mech. Phys. Solids* **49** 1209–37
[6] Mourad H M and Garikipati K 2006 Advances in the numerical treatment of grain-boundary migration: coupling with mass transport and mechanics *Comput. Methods Appl. Mech. Eng.* **196** 595–607
[7] Grychanyuk V, Tsukrov I and Gross T 2004 Numerical modeling of grain boundary effectis in the diffusional creep of copper interconnect lines *Int. J. Fract.* **127** L149–54
[8] Tsukrov I, Grychanyuk V M and Gross T S 2008 Finite element modeling of diffusional creep with explicit consideration of enhanced vacancy diffusivity in a finite region adjacent to the grain interface *Mech. Adv. Mater. Stuct.* **15** 533–9
[9] Gélébart L 2008 Micromechanical modelling of volume diffusion creep in a polycrystalline solid: a stress-diffusion coupled problem private communication

[10] Mishin Y, Warren J A, Sekerka R F and Boettinger W J 2013 Irreversible thermodynamics of creep in crystalline solids *Phys. Rev.* B **88** 184303
[11] Svoboda J, Fischer F D, Fratzl P and Kroupa A 2002 Diffusion in multi-component systems with no or dense sources and sinks for vacancies *Acta Mater.* **50** 1369–81
[12] Fischer F D and Svoboda J 2011 Chemically and mechanically driven creep due to generation and annihilation of vacancies with non-ideal sources and sinks *Int. J. Plast.* **27** 1384–90
[13] Fischer F D and Svoboda J 2010 Substitutional diffusion in multicomponent solids with non-ideal sources and sinks for vacancies *Acta Mater.* **58** 2698–707
[14] Svoboda J, Fischer F D and Fratzl P 2006 Diffusion and creep in multi-component alloys with non-ideal sources and sinks for vacancies *Acta Mater.* **54** 3043–53
[15] Barbe F, Forest S and Cailletaud G 2001 Intergranular and intragranular behavior of polycrystalline aggregates. Part 2: results *Int. J. Plast.* **17** 537–63 (*7th Int. Symp. on Plasticity and its Current Applications (Cancun, Mexico, January 1999)*)
[16] Sweeney C A, Vorster W, Leen S B, Sakurada E, McHugh P E and Dunne F P E 2013 The role of elastic anisotropy, length scale and crystallographic slip in fatigue crack nucleation *J. Mech. Phys. Solids* **61** 1224–40
[17] McDowell D L and Dunne F P E 2010 Microstructure-sensitive computational modeling of fatigue crack formation *Int. J. Fatigue* **32** 1521–42 (Emerging Frontiers in Fatigue)
[18] Geers M G D, Cottura M, Appolaire B, Busso E P, Forest S and Villani A 2014 Coupled glide-climb diffusion-enhanced crystal plasticity *J. Mech. Phys. Solids* **70** 136–53
[19] François D, Pineau A and Zaoui A 2012 *Mechanical Behaviour of Materials Solid Mechanics and its Applications*) (Dordrecht: Springer)
[20] Abrivard G, Busso E P, Forest S and Appolaire B 2012 Phase field modelling of grain boundary motion driven by curvature and stored energy gradients, part I: theory and numerical implementation *Phil. Mag.* **92** 3618–42
[21] Cheong K-S and Busso E P 2004 Discrete dislocation density modelling of single phase FCC polycrystal aggregates *Acta Mater.* **52** 5665–75
[22] Cahn J W and Larché F 1973 A linear theory of thermochemical equilibrium of solids under stress *Acta Metall.* **21** 1051–63
[23] Wilshire B and Battenbough A J 2007 Creep and creep fracture of polycrystalline copper *Mater. Sci. Eng.* A **443** 156–66
[24] Philibert J 1985 *Diffusion et Transport de Matière Dans les Solides* (Les Ulis: Éd de Physique)
[25] Balluffi R W, Allen S and Carter W C 2005 *Kinetics of Materials* (New York: Wiley)
[26] Ghosh R N 2013 Creep life predictions of engineering components: problems & prospects *Proc. Eng.* **55** 599–606 (*6th Int. Conf. on Creep, Fatigue and Creep-Fatigue Interaction*)
[27] Claire A D L and Rabinovitch A 1983 A mathematical analysis of diffusion in dislocations. III. Diffusion in a dislocation array with diffusion zone overlap *J. Phys. C: Solid State Phys.* **16** 2087
[28] Cottrell A 1975 *An Introduction to Metallurgy* 2nd edn Arnold E (London: Institute of Materials)
[29] Villani A, Busso E P, Ammar K, Forest S and Geers M G D 2014 A fully coupled diffusional-mechanical formulation: numerical implementation, analytical validation, and effects of plasticity on equilibrium *Archive Appl. Mech.* **84** 1647–64
[30] Kobayashi R, Warren J A and Carter W C 2000 A continuum model of grain boundaries *Physica* D **140** 141–50
[31] Abrivard G, Busso E P, Forest S and Appolaire B 2012 Phase field modelling of grain boundary motion driven by curvature and stored energy gradients. Part II: application to recrystallisation *Phil. Mag.* **92** 3643–64
[32] Balluffi R W and Mehl R F 1982 Grain boundary diffusion mechanisms in metals *Metall. Trans.* A **13** 2069–95
[33] Demkowicz M J, Hoagland R G, Uberuaga B P and Misra A 2011 Influence of interface sink strength on the reduction of radiation-induced defect concentrations and fluxes in materials with large interface area per unit volume *Phys. Rev.* B **84** 104102
[34] Capolungo L, Spearot D E, Cherkaoui M, McDowell D L, Qu J and Jacob K I 2007 Dislocation nucleation from bicrystal interfaces and grain boundary ledges: relationship to nanocrystalline deformation *J. Mech. Phys. Solids* **55** 2300–27
[35] Gifkins R C 1976 Grain-boundary sliding and its accommodation during creep and superplasticity *Metall. Trans.* A **7** 1225–32
[36] Millett P C, El-Azab A, Rokkam S, Tonks M and Wolf D 2011 Phase-field simulation of irradiated metals part I: void kinetics *Comput. Mater. Sci.* **50** 949–59

[37] Musienko A, Cailletaud G and Diard O 2004 Damage, opening and sliding of grain boundaries *IUTAM Symp. on Multiscale Modeling, Characterization of Elastic-Inelastic Behavior of Engineering Materials, Proc.* (*Solid Mechanics, its Applications* vol 114) ed S Ahzi pp 149–56 (*Int. Union Theoret & Appl Mech; Moroccan State Secretary Sci Res; Pacific NW Natl Lab; USA European Res Off; Univ Cadi Ayyad, FSSM; Univ Metz, UFR M I, Characterization of Elastic-Inelastic Behavior of Engineering Materials (Marrakech, Morocco, 20–25 October 2002)*)
[38] Wei Y J and Anand L 2004 Grain-boundary sliding and separation in polycrystalline metals: application to nanocrystalline fcc metals *J. Mech. Phys. Solids* **52** 2587–616
[39] Musienko A and Cailletaud G 2009 Simulation of inter- and transgranular crack propagation in polycrystalline aggregates due to stress corrosion cracking *Acta Mater.* **57** 3840–55
[40] Wilshire B and Palmer C J 2002 Grain size effects during creep of copper *Scr. Mater.* **46** 483–8
[41] Besson J, Cailletaud G, Chaboche J-L and Forest S 2010 *Non-Linear Mechanics of Materials* (Berlin: Springer)
[42] Thomas J P and Chopin C E 1999 Modeling of coupled deformation-diffusion in non-porous solids *Int. J. Eng. Sci.* **37** 1–24
[43] Lemaitre J and Chaboche J L 1994 *Mechanics of Solid Materials* (Cambridge: Cambridge University Press)